Stretch-induced intussuceptive and sprouting angiogenesis in the chick chorioallantoic membrane

Published in final edited form as:
Microvasc Res. 2014 September ; 95: 60–67. doi:10.1016/j.mvr.2014.06.009.

Stretch-induced Intussuceptive and Sprouting Angiogenesis in the Chick Chorioallantoic Membrane

Janeil Belle[1], **Alexandra Ysasi**[1], **Robert Bennett**[1], **Nenad Filipovic**[2], **Mohammad Imani Nejad**[3], **David L. Trumper**[3], **Max Ackermann**[4], **Willi Wagner**[4], **Akira Tsuda**[5], **Moritz A. Konerding**[4], and **Steven J. Mentzer**[1]

[1]Laboratory of Adaptive and Regenerative Biology, Brigham & Women's Hospital, Harvard Medical School, Boston MA

[2]Faculty of Mechanical Engineering, University of Kragujevac, Serbia

[3]Mechanical Engineering, Massachusetts Institute of Technology, Cambridge, MA

[4]Institute of Functional and Clinical Anatomy, University Medical Center of Johannes Gutenberg-University, Mainz, Germany

[5]Molecular and Integrative Physiological Sciences, Harvard School of Public Health, Boston, MA

Abstract

Vascular systems grow and remodel in response to not only metabolic needs, but mechanical influences as well. Here, we investigated the influence of tissue-level mechanical forces on the patterning and structure of the chick chorioallantoic membrane (CAM) microcirculation. A dipole stretch field was applied to the CAM using custom computer-controlled servomotors. The topography of the stretch field was mapped using finite element models. After 3 days of stretch, Sholl analysis of the CAM demonstrated a 7-fold increase in conducting vessel intersections within the stretch field ($p<0.01$). Morphometric analysis of intravital microscopy and scanning electron microscopy (SEM) images demonstrated that the increase vessel density was a result of an increase in interbranch distance ($p<0.01$) and a decrease in bifurcation angles ($p<0.01$); there was no significant increase in conducting vessel number ($p>0.05$). In contrast, corrosion casting and SEM of the stretch field capillary meshwork demonstrated intense sprouting and intussusceptive angiogenesis. Both planar surface area ($p<0.05$) and pillar density ($p<0.01$) were significantly increased relative to control regions of the CAM. We conclude that a uniaxial stretch field stimulates the axial growth and realignment of conducting vessels as well as intussusceptive and sprouting angiogenesis within the gas exchange capillaries of the *ex ovo* CAM.

Correspondence: Dr. Steven J. Mentzer, Room 259, Brigham &Women's Hospital, 75 Francis Street, Boston, MA 02115 smentzer@partners.org.

Introduction

Vascular systems grow and remodel in response to not only metabolic needs, but mechanical influences as well. Intraluminal forces, such as blood flow-induced changes in shear stress and circumferential stretch, are associated with local adaptations in vessel structure (Pries et al., 2005). Similarly, extravascular mechanical forces, such as the stretch associated with tissue growth and wound healing, have been associated with hypervascularity and small vessel angiogenesis (Lancerotto et al., 2012). These observations suggest that tissue-level mechanical forces can influence the structure and pattern of vascular networks.

In development, a variety of physical processes appear to stretch and fold tissues into mature structures (His, 1875). The mechanical stresses and strains associated with these processes have been recognized as relevant contributors to normal growth (Beloussov and Luchinskaia, 1995; Farge, 2011; Gjorevski and Nelson, 2010; Mammoto and Ingber, 2010). Most studies have investigated the in vitro effects of mechanical forces on cell processes such proliferation (Klein et al., 2009) and gene transcription (Mammoto et al., 2012). A few studies, unrelated to the microcirculation, have mechanically manipulated the tissue to clarify the influence of mechanical processes on growth. For example, a 10% lateral uniaxial deformation of Drosophila embryos resulted in expression of the morphogenetic protein Twist (Farge, 2003). Similarly, the modulation of morphogenic movements by laser pulses inhibited Drosophila development (Desprat et al., 2008).

In adult mammals, physical processes have been more commonly explored in the context of wound healing and tissue engineering. Tensile forces have been shown to stimulate cell proliferation as well as increased vessel diameter and density in the living skin (Erba et al., 2011a; Pietramaggiori et al., 2007). Microdeformational forces have been implicated in the enhanced angiogenic transcription associated with vacuum-assisted closure wound therapy (Erba et al., 2011b). Stretching the skin has been linked to angiogenic gene transcription and an increase in vessel density (Chin et al., 2010). Despite the apparent impact of mechanical forces on wound healing and tissue repair, the influence of stretch on microcirculatory architecture is largely unknown.

The chick chorioallantoic membrane (CAM) provides a unique opportunity to study the effect of uniaxial stretch on vascular architecture. The chick chorioallanotic membrane is a highly vascularized embryonic structure associated with the developing chick embryo after fusion of the chorion and allanotic layers between embryonic development day (EDD) 4 and 5 (Schlatter et al., 1997). *In ovo*, the CAM functions as a gas-exchange organ for the chick embryo. The accessibility of the CAM vasculature and quasi-planar characteristics of the CAM (approximately 20-100 μm thick) have supported its wide application in angiogenic and developmental research (Ribatti et al., 2001).

Here we have applied mechanical stretch force to the surface of EDD 10-13 CAMs over a 72 hour period. We found a differential response of conducting and capillary vessels. Most notably, we identified intense intussusceptive and sprouting angiogenesis in the CAM capillary meshwork.

Methods

Eggs

Pathogen-free fertilized White Leghorn chicken eggs (Gallus *domesticus*) were obtained from Charles River Laboratories (Wilmington, MA). Care was consistent with guidelines of the American Association for Accreditation of Laboratory Animal Care (Bethesda, MD) and approved by the Institutional Animal Care and Use Committee.

Ex ovo culture

For all experiments, a modified, ex ovo (shell-less) culture method was used for the Chick chorioallantoic membranes (CAM)(Dunn and Fitzharris, 1979). Briefly, the eggs were kept in a GQF digital incubator (GQF Manufacturing, Savannah, GA) at 37.5°C and 70% humidity with hourly automatic turning for 3 days. On embryonic development day (EDD) 3, the eggs were sprayed with 70% ethanol, air-dried in a laminar flow hood and explanted into a 20 x100 mm Petri dish (Falcon, BD Biosciences, San Jose, CA). The ex vivo cultures were maintained from EDD 3 to 14 in a humidified 2% CO_2 incubator at 37.5°C.

Mechanical stretch

A custom mechanical stretch apparatus was designed to apply uniaxial mechanical stretch to the cultured CAM. The stretch field was defined by two silk sutures (0.2mm, Perma-Hand, Ethicon) positioned 3.0 cm apart on the central CAM. One end of each suture was attached to the CAM surface with 2-octyl cyanoacrylate (Medline Industries, Mansfield, MA); the other end of each suture was coupled to a computer-controlled servomotor. The opposing servomotors were positioned to create a linear stretch field. In test CAM, pilot experiments suggested a maximal displacement rate of 0.034 mm/hr; control CAM, cultured in parallel, were coupled to stationary servomotors. Because of likely variability in initial suture tension, the stretch field was applied for 3 days to minimize the influence of initial conditions. For the duration of the experiment, the stretched (N= 356) and control (N=130) CAM were maintained in standard ex ovo culture conditions.

Intravital microscopy system

CAM vessels were visualized after intravascular perfusion with fluorescein-conjugated lycoperisicon esculentum (eBioscience,) and lens culinaris agglutinin lectins (Vector Laboratories Inc,). The fluorescent markers were injected into a CAM vessel using a 31-gauge insulin syringe (BD Biosciences, Franklin Lakes, NJ). The CAM microvasculature was imaged with using a Nikon SMZ-1000 stereoscope (0.5x Apo objective, 0.5x reduction lens) and Nikon FN1 epifluorescent microscope (Plan Fluor 4x, 10x objectives) fitted with heated (40.5°C) with a thermocontrol system (Tokai Hit, Japan). The Nikon stereoscope was configured for epifluorescent imaging using 470 nm LED illumination (Luxeon, Randolph, Vermont) and a custom-fit 515 nm long pass filter (Chroma, Rockingham, VT). A 480/40 nm excitation and 535/50nm emission filter set was used to visualize CAM vessels with the Nikon FN1 microscope. Fluorescent micrographs were recorded as 1040 x 770 pixel, 16-bit images using a 3 megapixel CCD camera (Jenoptik Progres Speed XT core, Jenoptik AG, Germany).

Sholl analysis

Sholl analysis was performed on fluorescent micrographs of stretch and control regions of the CAM microcirculation following digital exposure correction and image stitching using Adobe Photoshop CS5 (Adobe, San Jose, CA). Vessel distribution in stretch and control CAMs was evaluated using an adapted Sholl counting technique to enumerate vessels at varying distances from suture anchor points. (Gutierrez and Davies, 2007; Sholl, 1953). Similar to previous applications of the Sholl technique hierarchical trees and dichotomous branching vessels (Skoura et al., 2013; Strasser et al., 2010), a grid of concentric rings spaced 5 mm apart was centered over a suture anchor point on of the fluorescent micrograph of the CAM. Vessels intersecting the rings at 5, 10, and 15 mm were counted over a 3.5 cm^2 area of the CAM. Vessels located within a region extending radially from -60 to 60° from suture anchor point (centered at 0° of the stretch field) were included in analysis.

Image analysis

Analysis of still and video images was performed with MetaMorph 7.52 (Molecular Devices, Downingtown,PA) as previously described (Lee et al., 2011; Lee et al., 2010).The grayscale images were processed with standard MetaMorph filters. After routine thresholding, the image sequences were measured using MetaMorph's integrated morphometry and caliper applications. Morphometric measurements such as EDD 10-14 embryo and CAM surface area, and CAM perimeter were calculated using serial, distance-calibrated images of the ex ovo CAM obtained orthogonal to the CAM surface.

Vessel interbranch distance and branching angle were similarly measured with digital morphometry applications and fluorescent micrographs. Interbranch distance was defined as the length of the vessel segment between two vessel branch points. Vessel branch angles were measured as the angle between two branching vessel segments Capillary plexus fractional area was calculated as the proportion of pixels representing capillary plexus vasculature in binarized, high resolution SEM images. Pillar density in the SEM images was determined after counting the number of intravascular pillars (intravascular channel or “hole”-like structures less than 2.0 μm) present in 100 μm^2 grid area. The pillar number per 100 μm^2 is reported after adjusting for capillary plexus density.

Finite element modeling

Two finite element models were developed. First, the CAM was treated as a linear elastic uniform material of E = 50 MPa (Young's modulus) and ν = 0.49 (Poisson's ratio). Second, the CAM was treated as a combination of two different linear elastic materials; one is the same as baseline model, E = 50 MPa and ν = 0.49, and the other with slightly stiffer material E = 50 GPa & ν = 0.49, representing an embryo. The outer perimeters of the system in both cases were fixed, mimicking petri dish walls. In both cases, the system was discretized into 6782 2D four-node finite elements using unstructured discretization. The outer external tension T (5,000 N each) were applied to the system at Point A and B, representing tensional forces applied on the CAM by the sutures attached to the CAM surface.

CAM corrosion casting

Using a 27 gauge needle, the CAM vasculature was flushed with 2ml of 37°C PBS and fixed with 2ml of buffered 2.5% glutaraldehyde. A 5:3.5:1 resin mixture of PU4ii polyurethane elastomer (vasQtec, Zurich, Switzerland), 2-butanone, and Pu4ii resin hardener, (vasQtec, Zurich, Switzerland) was injected into CAM vessels. After polymerization at 25°C, the CAM tissue was excised and macerated in 5% potassium hydroxide solution, and coated with gold in an argon atmosphere prior to imaging with a Philips ESEM XL30 scanning electron microscope.

CT scanning

The CT scanner (GE explore VISTA, GE Healthcare, Waukesha, WI, USA) was set to a potential of 40kV and a current of 140 μA. In some scans, the CAM surface imaging was aided by the application of topical 40% barium sulfate (Sigma-Aldrich, St Louis, MO). Margins of the Petri dish were defined, and the CAM images were obtained at standard resolution (50 μm/slice).

Statistical analysis

Significance estimates were based on multiple comparisons of paired data by Student-Newman-Keuls or Mann-Whitney test for non-parametric analysis of variance. Pearson correlations to the unamplified control were determined using Systat 12 statistical software (Chicago, IL).The significance level for the sample distribution was defined as $p<0.05$.

Results

Ex ovo CAM development

The explanted eggs were studied between 10 and 13 of the 21 day chick development period. In *ex ovo* culture conditions, the CAM surface area varied from 55.92 ± 1.73 cm^2 on day 10 to 41.42 ± 1.78 cm^2 on day 14. In contrast, the embryo planar surface area (2D projection) increased from $4.15 + 0.15$ cm^2 on day 10 to 8.53 ± 0.36 cm^2 on day 14 (Figure 1). CAM and embryo growth—and perhaps culture conditions—resulted in positional changes of vessel segments throughout the study period; the median change was 3.11 mm.

Dipole stretch

To investigate the influence of micromechanical forces on the CAM vascular microarchitecture, we applied uniaxial stretch by adhering 2 surgical sutures to the CAM surface (Figure 2A,B). Constant load uniaxial traction was applied to the sutures using two opposing microprocessor-controlled motors mounted to a custom platform (Figure 2A,B). The stretch platform was modifiable to insure that traction was applied parallel to the CAM surface thereby avoiding Z-axis surface deformation. Of note, microCT scans of the CAM demonstrated contour (Z-axis) variation of less 5% in the stretch field (not shown). In preliminary experiments, the maximal tolerated stretch was estimated by applying variable uniaxial stretch for 1, 2 or 3 days. The maximum displacement rate associated with rare membrane disruption was 0.034 mm/hour; this rate was applied in subsequent experiments. Application of the static stretch (0.808 mm/24 hours) for 3 days resulted in suture

displacement of 2.33 ± 0.51 cm compared to 0.02 ± 0.44 cm in the control CAM ($p<0.001$) (Figure 2D). There was relatively constant CAM surface area and perimeter in both stretch and control CAM ($p>0.05$)(Figure 2E-F).

Finite element model of stretch field

To define the stretch field, finite element (FE) modeling was performed assuming a uniform linear elastic medium (Figure 3A-C) as well as a nonuniform linear elastic medium to simulate the presence of an embryo (Figure 3D-F). The uniform FE models demonstrated a rapid decrease in displacement from the point of external force application (Figure 3B). Similarly, the FE models of the CAM stress demonstrated maximal stress at the point of attachment, but also a linear stress band between the points of attachment—a band that defined the “stretch field” (Figure 3C). The non-uniform FE models demonstrated a contour map with the gradient displacement remote from the embryo (Figure 3E). This finding suggested that the CAM deformation is very sensitive to the membrane's mechanical properties. The stress map, consistent with a stiffer material being the loadbearing element, demonstrated significant stress on the “embryo” in our models (Figure 3F).

Stretch effects on the conducting vessels

To assess the architecture of the conducting vessels at the conclusion of the stretch period, we analyzed the stretch field using fluorescent intravital microscopy and Sholl analysis (Sholl, 1953). The Sholl profile reflected the number of vascular intersections within radial sectors originating at the attachment point (Figure 4A,B; grid overlay). The number of vascular intersections within the stretch field (-20° to +20°) was significantly greater in the stretched CAM (58.8 ± 28.3) than in the control CAM (8.1 ± 3.9)($p<0.01$; Figure 4C,D). Higher resolution intravital microscopy as well as corrosion casting and SEM demonstrated that the increase in vascular density primarily reflected re-alignment and lengthening of 1^{st} through 4^{th} order conducting vessels. Quantitative morphometry of these conducting vessels demonstrated no increase in conducting vessel number ($p> 0.05$), but an increase in interbranch distance (2.63 ± 0.58 mm stretch and 0.99 ± 0.33 mm controls, $p<0.01$)(Figure 5A,B) as well as a decrease in bifurcation angles (30.8 ± 6.9° stretch and 69.2 ± 16.9° controls, $p<0.01$)(Figure 5C,D) within the stretch field.

Stretch effects on the capillary meshwork

To assess the stretch effects on the capillary plexus, we used corrosion casting and scanning electron microscopy. Corrosion casts demonstrated distinct changes within the stretch field. SEM confirmed the increase in conducting vessel interbranch distance and the decrease in vessel angle. Notably, the stretch field demonstrated a remarkable increase in capillary density associated with both capillary sprouts and intussusceptive pillars (Figure 6). Morphometric analysis demonstrated a significant increase in capillary density as measured from a 2D (planar) projection ($p<0.05$)(Figure 7A,B). In addition, the stretch field demonstrated a marked increase in the number of pillars when compared to control CAM ($p<0.01$)(Figure 7C,D). Interestingly, paired pillars were frequently observed within the stretch field (Figure 7C, ellipses).

Discussion

In this report, we investigated the influence of mechanical stretch on the vascular architecture of the CAM microcirculation. After applying continuous uniaxial stretch between EDD 10 and 13, we observed 1) re-alignment of the conducting vessels parallel to the stretch field reflected by a marked decrease in branch angles, 2) an increase in axial length of the conducting vessels within the stretch field manifested by a significant increase in interbranch distance, and 3) a dramatic increase in both sprouting and intussusceptive angiogenesis in the capillary meshwork demonstrated by corrosion casting and SEM. The data indicate that mechanical stretch can be a potent stimulus for adaptive modification of microcirculatory architecture. Further, the distinct responses of the conducting and capillary vessels within the same stretch field suggest that tissue-level mechanical forces have vessel-specific effects within the vascular network.

Our observations of stretch-induced vascular morphology and angiogenesis occur in the *ex ovo* CAM culture model by which the CAM may be studied as a quasi-planar vascular tissue. Embryo and CAM growth under *ex ovo* conditions varies from normal growth, as the position of the embryo and CAM are rearranged and growth of these components may be affected by the boundary conditions of the culture dish which appears to influence growth beyond EDD 13.The stretch field produced a marked change in the topography of the microcirculation. Within 24 hours, conducting vessels within the stretch field were oriented parallel to the stretch axis. This topographic re-alignment was reminiscent of the typical “starburst” or “spoke-and-wheel” vascular pattern noted in many studies of CAM angiogenesis. The change in vascular topography was not simply traction-induced distortion of the membrane as the overall CAM surface area and the vessels outside of the stretch field appeared similar to control (unstretched) CAM. The observed vessel pattern also was not a consequence of vessel replication as the number of 2^{nd}, 3^{rd}, and 4^{th} order vessels—those vessels most readily identifiable by light and fluorescence microscopy—did not increase. In this experimental design, the topographic changes were a result of a decrease in branch angle (mean branch angle less than 20 degrees) and a 2.5-fold increase in interbranch distance; that is, the topographic changes were primarily a result of the re-alignment and axial growth of the conducting vessels.

The most intriguing observation was the dramatic angiogenesis within the capillary plexus. Corrosion casting and SEM demonstrated morphologic changes including obliteration of the fine capillary meshwork by densely matted capillaries with confluent areas of active sprouting and intussusceptive angiogenesis. Most notable was the density and distribution of intussusceptive pillars—that is, the transluminal tissue bridges that characterize the early stages of the process of intussusceptive angiogenesis (De Spiegelaere et al., 2012; Djonov et al., 2000). Not only were innumerable pillars seen in the growing capillary network, but uncommon features such as paired and incomplete pillars were observed. Because of the re-alignment of the conducting vessels, these changes in the capillary meshwork were not observed by fluorescence microscopy; the active angiogenic sprouts and intussusceptive pillars were best seen using corrosion casting and SEM.

The temporal and spatial coincidence of capillary sprouts and intussusceptive pillars suggests that stretch is a common trigger for both types of angiogenesis. Previously, Konerding et al. have suggested that the distinction between these processes was the orientation of the endothelial cell—extraluminal migration in sprouting angiogenesis and intraluminal migration in intussusceptive (nonsprouting angiogenesis)(Konerding et al., 2010). More recent work suggests other important distinctions between sprouting and intussusceptive angiogenesis (Mentzer and Konerding, 2014); nonetheless, the stretched CAM provides a unique opportunity to define these similarities and differences.

A more general observation in our studies was the sensitivity of the CAM to mechanical distortion—whether the distortion was traction parallel to, or depression of, the CAM surface. Depression of the CAM surface, typically by the weight of a ring or graft, can result in a “starburst” vascular pattern independent of any additional angiogenic stimulus. For this reason, we minimized the amount of adhesive and meticulously ensured that the stretch field was parallel to the CAM surface.

An assumption of these studies was the homogeneity of the stretch field. Although the external load on the membrane was reproducible, the internal forces could theoretically vary considerably both between and within CAM. For example, it is possible that the vessel-specific responses to stretch reflected differential strain; that is, it is possible that the conducting vessels were the dominant stress-bearing element within the membrane and that the capillary meshwork was exposed to only a fraction of the strain. While a heterogeneous stretch field is possible, we believe it is unlikely to account for the different responses of the conducting vessels and capillary meshwork. Although the initial conducting vessel architecture was variable between CAM, the final pattern of conducting vessels was similar—an observation that suggests the stretch field, not conducting vessel architecture, determined the adaptive changes in the network. Moreover, we applied a constant stretch field over 3 days to ensure a reproducible stretch signal. The results of these studies have encouraged us to pursue stretch protocols more likely to produce inhomogeneities in the stretch field—such as the application of cyclic and/or biaxial stretch.

In this study, the “stretch field” reflected both practical and theoretical concepts. From a practical viewpoint, the finite element modeling provided a topographic map of both the intensity and distribution of chorioallantoic membrane displacement and strain; that is, a map of the stretch field. From a theoretical viewpoint, the concept of a “stretch field” also reflected the integrated response of the CAM microcirculation—as a structural system—to mechanical signals. Stretch produced distinct responses in different components of the microcirculation; that is, conducting vessels changed their alignment and increased their length, whereas the gas-exchange beds—the capillary meshwork—underwent dramatic multiplicative angiogenesis in response to stretch. In this latter sense, the “stretch field” reflected the informational and spatial relationships relevant to an adaptive response of the regional microcirculation. As suggested by this field model, future experiments will necessarily require both vessel-specific spatial sampling as well as an architecture-aware approach to interpreting these findings.

Acknowledgments

Supported in part by NIH Grant HL95678

Abbreviations

2D	2-dimensional
3D	3-dimensional
CAM	chick chorioallantoic membrane
EED	embryonic development day
FE	finite element
SEM	scanning electron microscopy

References

Beloussov LV, Luchinskaia NN. Biomechanical feedback in morphogenesis, as exemplified by stretch responses of amphibian embryonic tissues. Biochem. Cell Biol. 1995; 73:555–563. [PubMed: 8703426]

Chin MS, et al. In vivo acceleration of skin growth using a servo-controlled stretching device. Tissu Eng. Pt. C-Meth. 2010; 16:397–405.

De Spiegelaere W, et al. Intussusceptive angiogenesis: A biologically relevant form of angiogenesis. J. Vasc. Res. 2012; 49:390–404. [PubMed: 22739226]

Desprat N, et al. Tissue deformation modulates twist expression to determine anterior midgut differentiation in Drosophila embryos. Dev. Cell. 2008; 15:470–477. [PubMed: 18804441]

Djonov V, et al. Intussusceptive angiogenesis: its role in embryonic vascular network formation. Circ. Res. 2000; 86:286–92. [PubMed: 10679480]

Dunn BE, Fitzharris TP. Differentiation of the chorionic epithelium of chick-embryos maintained in shell-less culture. Dev. Biol. 1979; 71:216–227. [PubMed: 499657]

Erba P, et al. A morphometric study of mechanotransductively induced dermal neovascularization. Plastic and Reconstructive Surgery. 2011a; 128:288–299.

Erba P, et al. Angiogenesis in wounds treated by microdeformational wound therapy. Ann. Surg. 2011b; 253:402–409. [PubMed: 21217515]

Farge E. Mechanical induction of twist in the Drosophila foregut/stomodeal primordium. Curr. Biol. 2003; 13:1365–1377. [PubMed: 12932320]

Farge, E. Forces and Tension in Development. Vol. 95. Elsevier Academic Press Inc; San Diego: 2011. Mechanotransduction in development.; p. 243-265.

Gjorevski N, Nelson CM. The mechanics of development: Models and methods for tissue morphogenesis. Birth Defects Res. Part C-Embryo Today-Rev. 2010; 90:193–202.

Gutierrez H, Davies AM. A fast and accurate procedure for deriving the Sholl profile in quantitative studies of neuronal morphology. J. Neurosci. Methods. 2007; 163:24–30. [PubMed: 17367866]

His, W. Unsere Körperform und das physiologische Problem ihrer Entstehung : Briefe an einen befreundeten Naturforscher. F.C.W. Vogel; Leipzig: 1875.

Klein EA, et al. Cell-cycle control by physiological matrix elasticity and in vivo tissue stiffening. Curr. Biol. 2009; 19:1511–1518. [PubMed: 19765988]

Konerding MA, et al. Inflammation-induced intussusceptive angiogenesis in murine colitis. Anat. Rec. 2010; 293:849–857.

Lancerotto L, et al. Mechanisms of action of microdeformational wound therapy. Semin. Cell Dev. Biol. 2012; 23:987–992. [PubMed: 23036531]

Lee GS, et al. Intravascular pillars and pruning in the extraembryonic vessels of chick embryos. Dev. Dyn. 2011; 240:1335–1343. [PubMed: 21448976]

Lee GS, et al. Blood flow shapes intravascular pillar geometry in the chick chorioallantoic membrane. J. Angiogenes. Res. 2010; 2:11–20. [PubMed: 20609245]

Mammoto A, et al. Mechanosensitive mechanisms in transcriptional regulation. J. Cell Sci. 2012; 125:3061–3073. [PubMed: 22797927]

Mammoto T, Ingber DE. Mechanical control of tissue and organ development. Development. 2010; 137:1407–1420. [PubMed: 20388652]

Mentzer SJ, Konerding MA. Intussusceptive angiogenesis: Expansion and remodeling of microvascular networks. Angiogenesis. 2014 In press.

Pietramaggiori G, et al. Tensile forces stimulate vascular remodeling and epidermal cell proliferation in living skin. Ann Surg. 2007; 246:896–902. [PubMed: 17968184]

Pries AR, et al. Remodeling of blood vessels: responses of diameter and wall thickness to hemodynamic and metabolic stimuli. Hypertension. 2005; 46:725–31. [PubMed: 16172421]

Ribatti D, et al. Chorioallantoic membrane capillary bed: A useful target for studying angiogenesis and anti-angiogenesis in vivo. Anat. Rec. 2001; 264:317–324. [PubMed: 11745087]

Schlatter P, et al. Quantitative study of intussusceptive capillary growth in the chorioallantoic membrane (CAM) of the chicken embryo. Microvasc. Res. 1997; 54:65–73. [PubMed: 9245646]

Sholl DA. Dendritic organization in the neurons of the visual and motor cortices of the cat. J. Anat. 1953; 87:387–406. [PubMed: 13117757]

Skoura A, et al. Analyzing tree-shape anatomical structures suing topological descriptors of branching and ensemble of classifiers. J. Theoret. Appl. Comp. Sci. 2013; 7:3–19.

Strasser GA, et al. Microarray analysis of retinal endothelial tip cells identifies CXCR4 as a mediator of tip cell morphology and branching. Blood. 2010; 115:5102–5110. [PubMed: 20154215]

Highlights

- A defined stretch field was applied to the chick chorioallantoic membrane
- Stretch-induced angiogenesis was demonstrated a marked increase in vessel density.
- Conducting vessels demonstrated axial growth and diminished bifurcation angles.
- The capillary network demonstrated dramatic intussusceptive and sprouting angiogenesis.

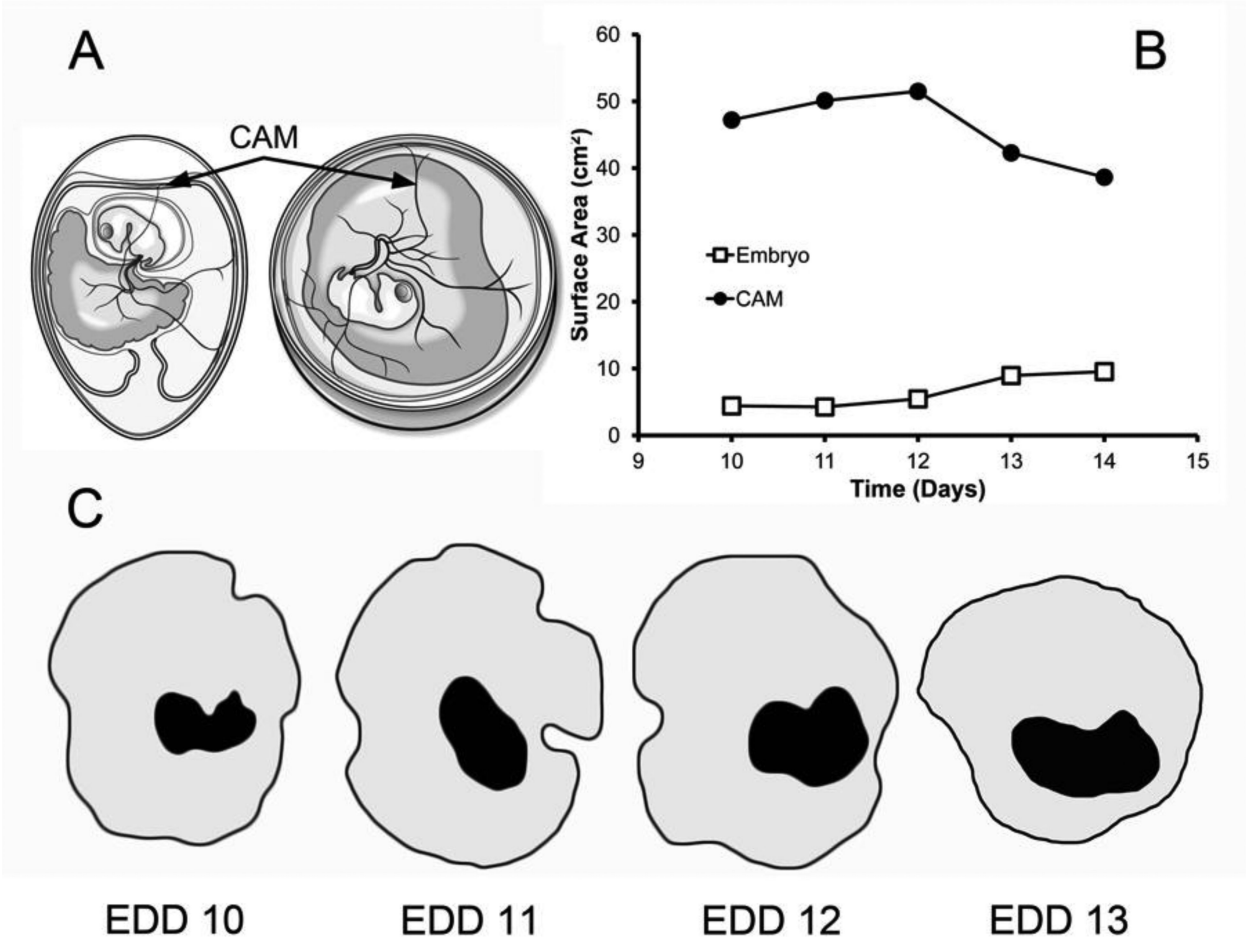

Figure 1.

Schematic diagram of the chick chorioallantoic membrane (CAM) *in ovo* and after explantation (A). The change in CAM and embryo surface area (planar projection) in a representative ex ovo culture specimen is shown in B. The quasi-planar surface of a representative CAM is shown (planar projection) in C.

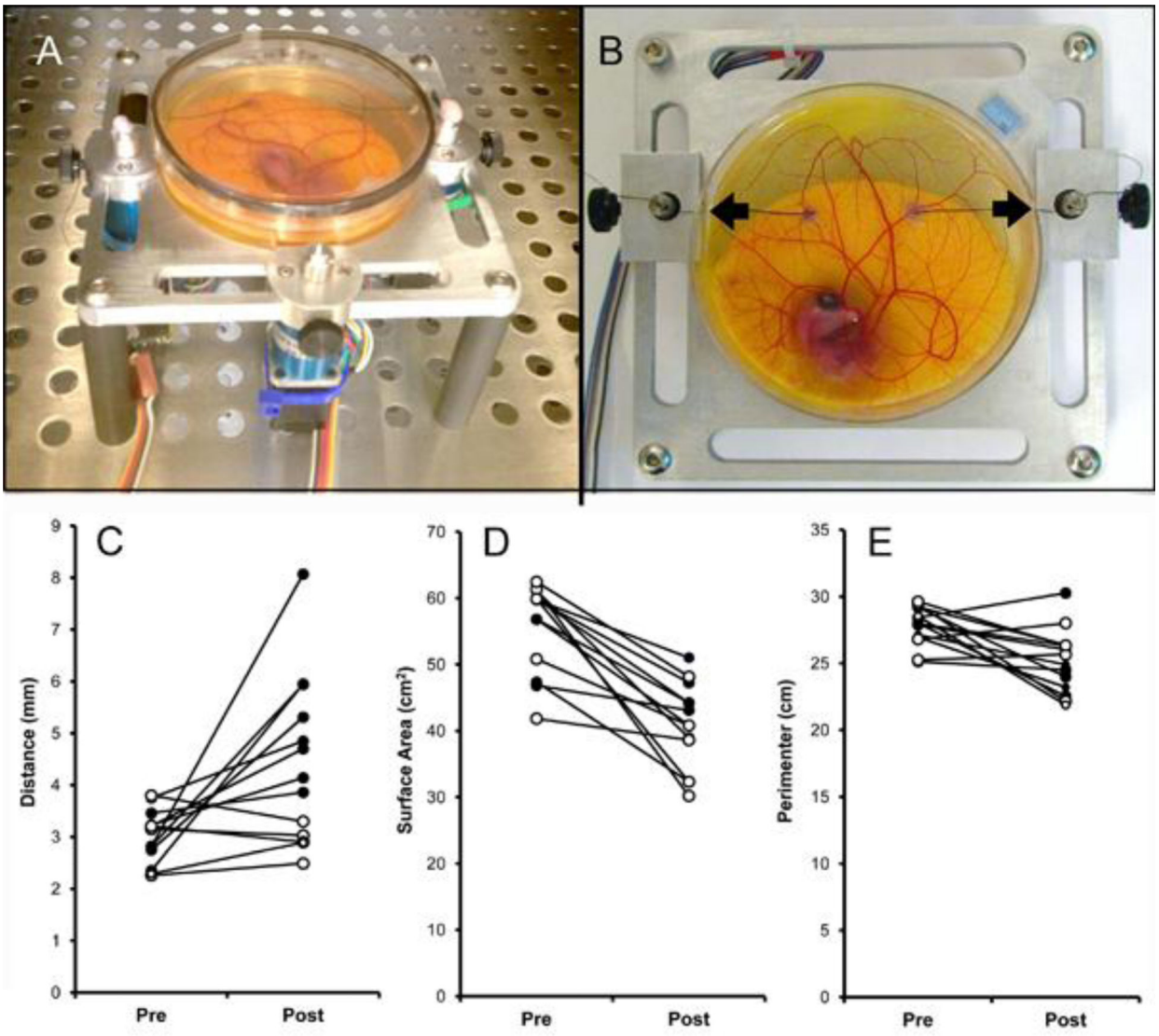

Figure 2.

The stretch apparatus (A,B) used to apply the stretch field. B) Sutures attached to the EDD 10 chorioallantoic membrane (CAM) produced a uniaxial stretch field (black arrows); in control CAMs, the sutures were coupled to stationary motors. C) The result of the stretch field was a significant displacement of the suture attachment point in test CAMs ($p<0.05$) (stretch, closed circles; control, open circles). There was no significant difference in CAM surface area (D) or perimeter (E)($p>0.05$, N=12).

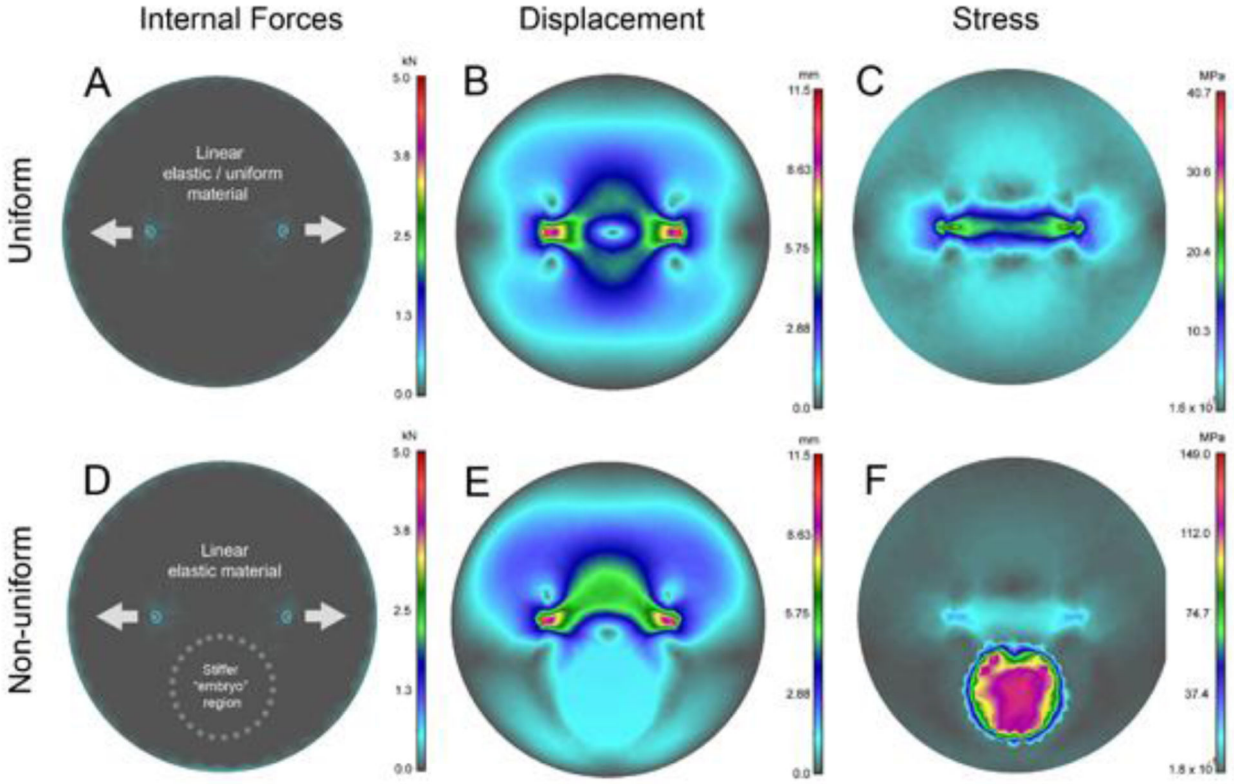

Figure 3.

Finite element models of the CAM stretch field. The Petri dish is assumed to reflect a static boundary; that is, these numerical simulations assumed that the shape of the CAM did not change. Internal forces (A,D) were assumed to be negligible. The simulations indicated modest displacement of the attachment points (B) with a linear stretch field reflected by the stress contour (C). The modification of the simulation to include a stiffer region of the CAM (D)—reflecting the presence of an embryo—had a moderate effect on both the displacement and stress contours (E,F). Of note, there was a prominent stress contour in the region of the "embryo" (F).

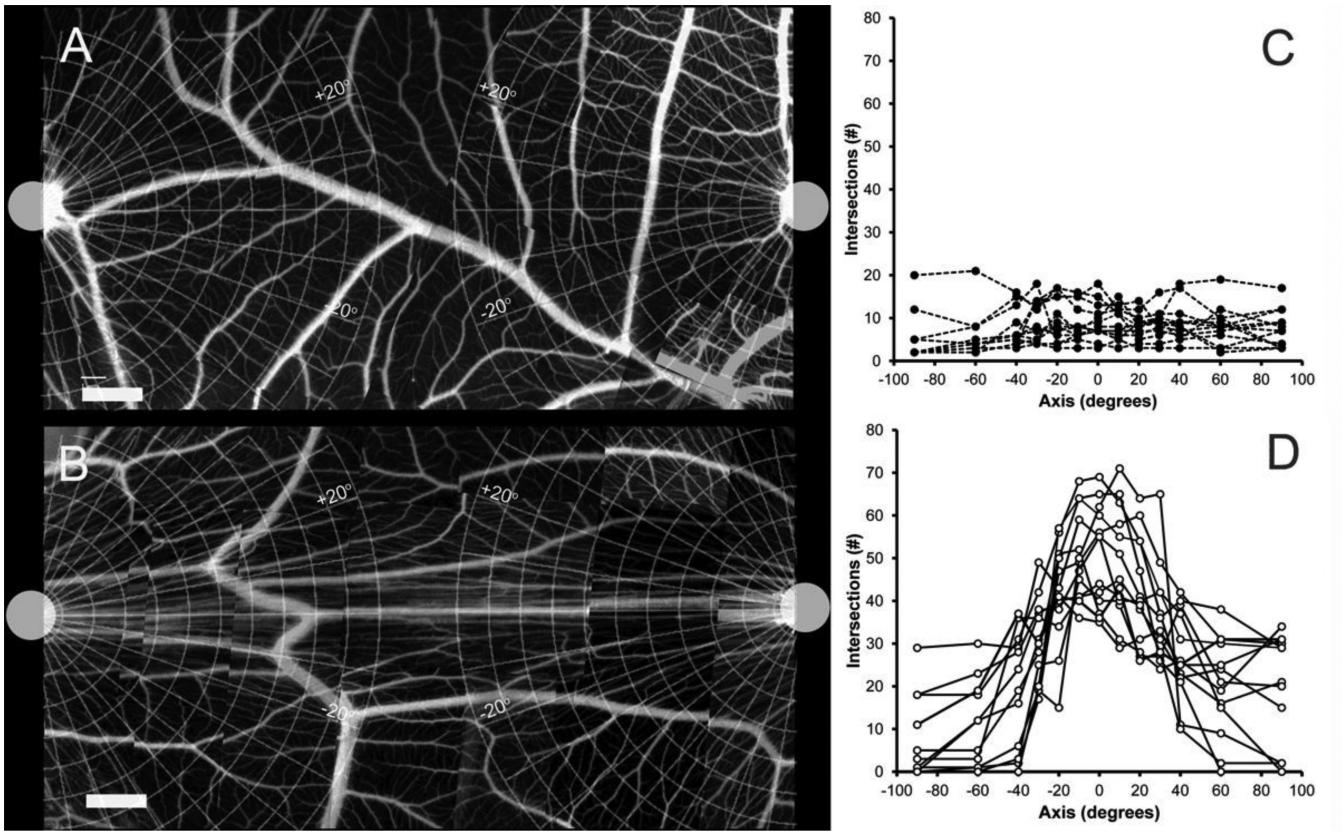

Figure 4.

Sholl analysis of mosaic image reconstructions of the vascular pattern after 3 days (EDD 10 to 13) of stretch. Control CAM, with attachment points (circles) coupled to stationary servomotors, demonstrated little re-alignment of the CAM vessels (A,C). B) Test CAM stretched for 3 days demonstrated marked re-alignment of the conducting vessels within the stretch field (B,D). Variation in vessel location reflects normal CAM movements; variation in intravascular fluorescence reflects the time-dependent perfusion differences during multi-image acquisition. In panels C and D, closed circles are Sholl intersections in control CAM (N=7); open circles are Sholl intersections in CAM after 3 days of stretch (N=8). Radial sectors from -20° to +20° are indicated on the Sholl grid; bar =3mm.

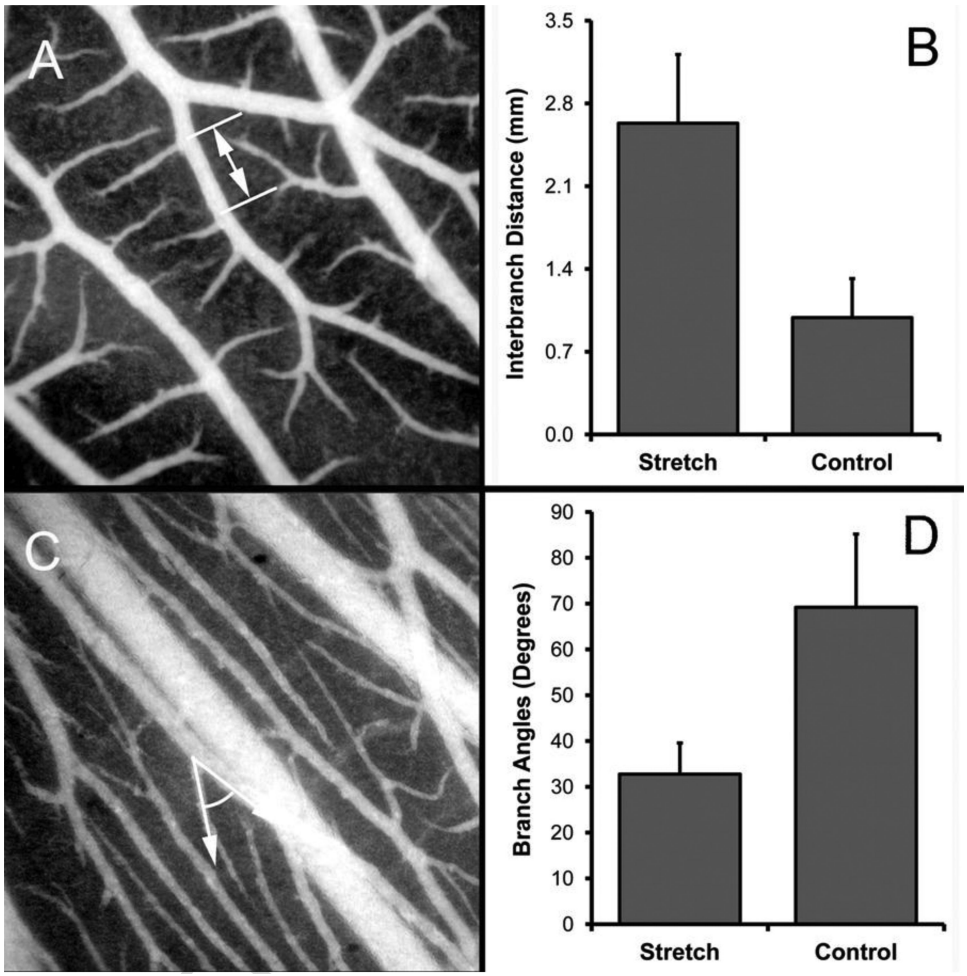

Figure 5.

Morphometry of the microcirculation in control (A) and stretched (C) CAM studied by fluorescence intravital microscopy of the stretch field. B) Interbranch distance was significantly greater in the stretch field than in controls ($p<.05$). D) Similarly, vessel branch angles were significantly decreased in the stretch field ($p<.05$)($N=15$).

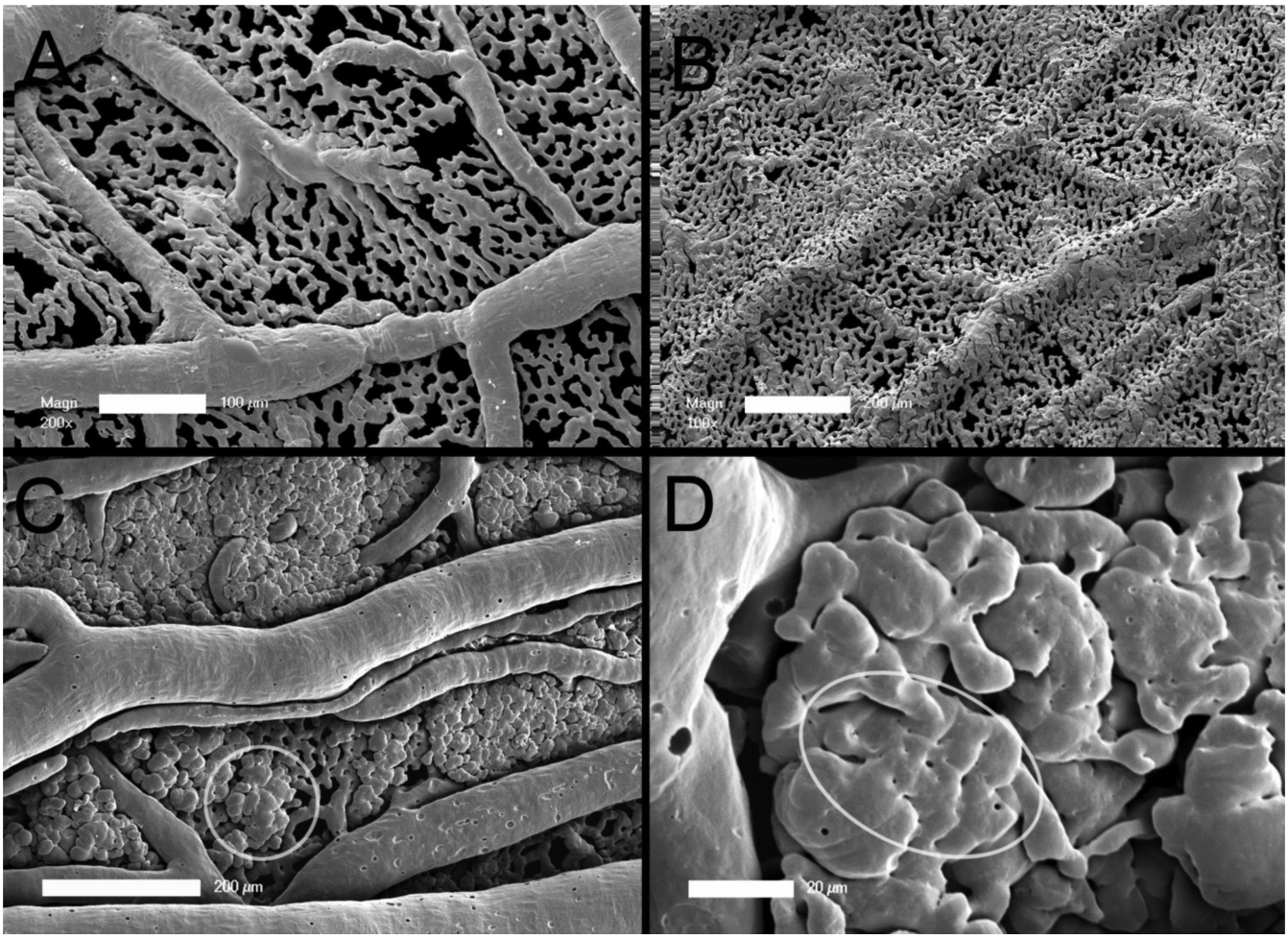

Figure 6.

Corrosion casting and scanning electron microscopy (SEM) of the EDD 13 CAM microcirculation. Control CAM microcirculation demonstrated a delicate capillary meshwork observed from the conductive vessel (A) and capillary (B) surfaces. After the application of stretch for 3 days (EDD 10 to 13), the capillary meshwork demonstrated confluent growth of the network (C) with morphologic evidence of both sprouts and many intussusceptive pillars (D, ellipse).

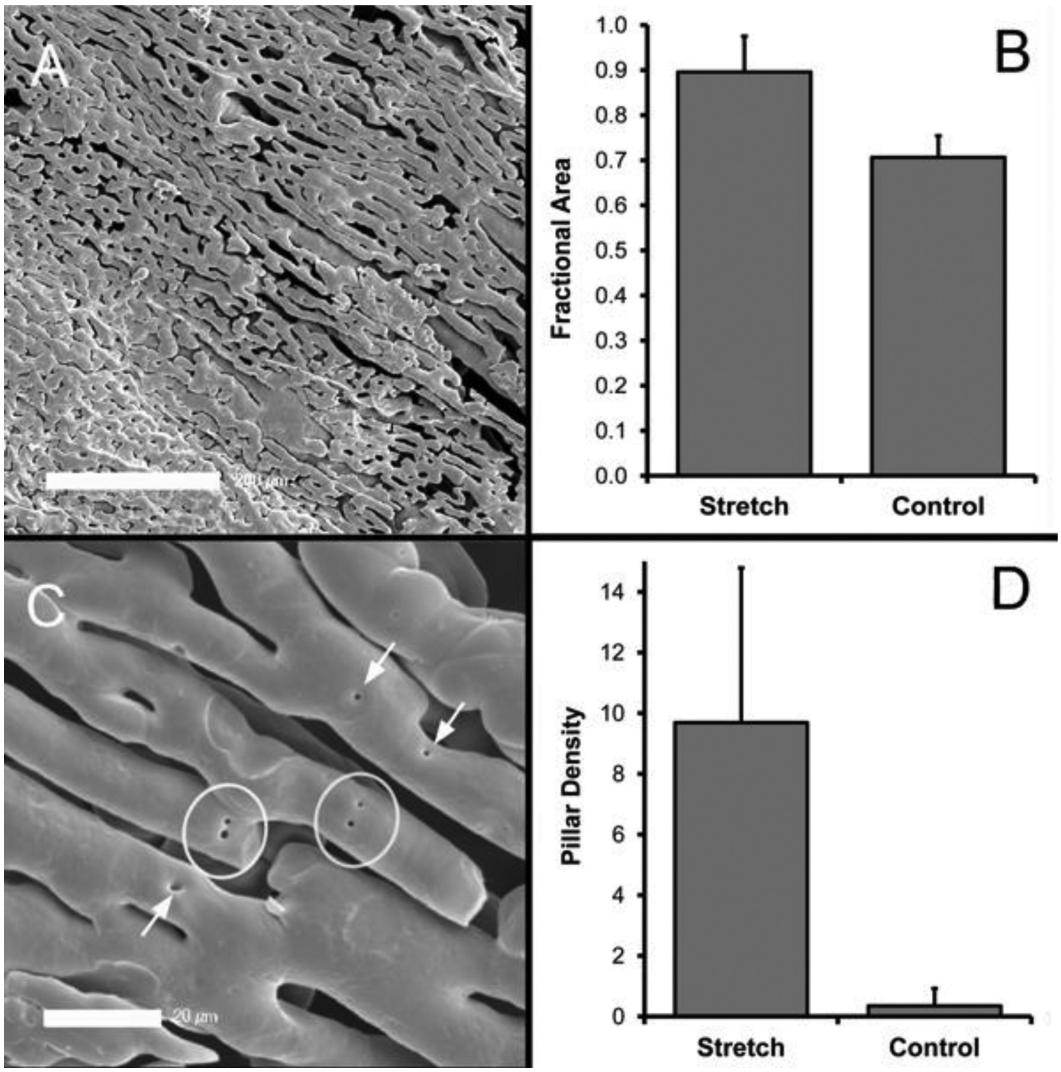

Figure 7.

Corrosion casting and scanning electron microscopy (SEM) of the EDD 13 CAM stretch field. Planar (2D) projections of the stretch field (A) were imaged; vessels were thresholded and surface area was calculated using morphometry software (MetaMorph). B) The fractional surface area was significantly greater in stretched compared to control CAM ($p<.05$). C) Higher resolution SEM demonstrated small pillars (arrows) often seen as doublets (ellipses). D) The number of pillars, expressed per 100μm^2 was significantly higher in stretched CAMs compared to controls (N=6; $p<.01$).